Primary Processes and Structure of the Photosystem II Reaction Center. 3. Kinetic Analysis of Picosecond Energy Transfer and Charge Separation Processes in the D1−D2−cyt-b559 Complex Measured by Time-Resolved Fluorescence†

Guido Gatzen,‡ Marc G. Müller, Kai Griebenow, and Alfred R. Holzwarth*

Max-Planck-Institut für Strahlenchemie, Stiftstrasse 34−36, D-45470 Mülheim a.d. Ruhr, Germany

Received: October 19, 1995; In Final Form: January 31, 1996⊗

An extensive picosecond fluorescence study has been performed on isolated D1−D2 reaction centers (RCs) from photosystem (PS) II at room temperature as a function of excitation and emission wavelength with a time resolution of about 2 ps. The study comprizes more than 50 excitation/emission wavelength pairs. Global analysis for individual excitation wavelengths and, alternatively, for the entire excitation/emission wavelength matrix has been performed. These analyses show that over a time range of 2 ns five exponentials are required to adequately describe the data. The shortest lifetime component, whose amplitude dominates the excited state decay for excitation in the red part of the absorption spectrum, is ≈3 ps. Further lifetime components fall into the 6−12, 20−30, and 60−130 ps and the several nanosecond ranges. In the combined global analysis at least five lifetime components (400 ps fit window), again with ≈3 ps as the shortest one (again dominant in amplitude for long excitation wavelengths), and most likely even six components are required to describe the data. The dominance and necessity of the ≈3 ps component is demonstrated also by exhaustive search error analysis on the data in the global mode. Kinetic target analysis on models of various complexity has been performed, again on data sets from individual excitation wavelengths and on the combined data set. Such analyses have been performed for the first time for the D1−D2 kinetics, and they allow an assignment of the origin of the various lifetime components. The target analyses yielded realistic species-associated spectra (SAS), as expected for Chl excited states and also the rate constants for the energy transfer and charge separation processes. The results show that (i) the majority of the *effective* primary charge separation is associated with the ≈3 ps lifetime, (ii) three pools of external Chls, transferring their energy relatively slowly to the RC core, are attached to the D1−D2 RC, (iii) the three Chls have energy transfer times in the range of 6−30 ps, and (iv) a ≈50 ps component is associated with a transition between different radical pairs. We exclude on the basis of these data that the primary charge separation could occur primarily in 21 ps, as proposed by other authors (Durrant; et al. *Biochemistry* **1993**, *32*, 8259−8267). In all models, quite independent of their complexity, the effective primary charge separation rate (from the equilibrated RC core) is in the range of 100−150 ns^{-1}. If one accounts for the distribution of the excited state in the RC core over various chromophores an *intrinsic* charge separation rate constant from P680* to the primary radical pair can be estimated to be ≈360 ns^{-1}, corresponding to an intrinsic charge separation lifetime of ≈2.7 ps, in very good agreement with our previous extrapolation based on the kinetics of intact PS II core particles (Schatz; et al. *Biophys. J.* **1988**, *54*, 397−405). It is concluded that the intrinsic primary charge separation in isolated D1−D2 reaction centers has about the same rate constant as in intact photosystem II.

Introduction

Photosystem II (PS II) is the pigment−protein complex in the thylakoid membrane of higher plants that is responsible for oxygen evolution.[1] Its reaction center (RC), the so-called D1−D2−cyt-b559 complex, has been isolated for the first time now nearly 10 years ago.[2,3] In isolated form this pigment−protein complex consists of the D1 and D2 polypeptides and the apoproteins of cytochrome *b*-559.[2,4,5] The D1 and D2 polypeptides of the PS II RC complex have significant homology with the L and M subunits of bacterial RCs, respectively.[6−8] In contrast to bacterial RCs, the absorption spectrum of the D1−D2−cyt *b*-559 complex is dominated by a strong spectral congestion of the Q_y-bands of all pigments, in combination with a substantial inhomogeneous broadening of pigment absorption bands. This inhomogeneous broadening and the homogeneous broadening at room temperature are of the same order or, for some chromophores, even larger than the spectral separation of the individual pigments.[9,10] These two factors seriously hamper all optical spectroscopic studies and provide severe difficulties for the elucidation of the energy level ordering in PS II RCs.[4,11−13] In a recent study Konermann et al. presented a detailed analysis and interpretation of the D1−D2 absorption spectrum, based on calculated line shapes of individual pigments, taking into account electron−phonon coupling and inhomogeneous broadening.[10]

The pigment content of D1−D2 complexes has recently been a matter of debate.[10,14−16] However, at present there seems to be an agreement between most groups, that most stable preparations contain at least 6 chlorophyll (Chl)/2 pheophytin (Pheo) but often ranging up to seven or more Chl/2 Pheo. Most typical preparations obtained in various laboratories range between 6.3 Chl/2 Pheo and 6.7 Chl/2 Pheo. Konermann and

* To whom all correspondence should be addressed.

† This work has been presented in part at the ESF-Workshop on "Structure and Function of the isolated D1−D2 reaction center", Wye College, England, April 1995, and at the workshop on "Electron transfer processes in photosynthesis and artificial systems", Jyväskylä, Finland, November 1994.

‡ This work is part of the Ph.D. Thesis of G.G. at the Heinrich-Heine-Universität, Düsseldorf, Germany.

⊗ Abstract published in *Advance ACS Abstracts,* April 1, 1996.

0022-3654/96/20100-7269$12.00/0 © 1996 American Chemical Society

Holzwarth[10] recently proposed that typically D1−D2 preparations contain Chl in a nonstoichiometric ratio, i.e., that typical preparations are mixtures of particles with different Chl contents. In that study also a detailed correlation of the absorption spectrum with the exact pigment content was presented, indicating the presence of several Chl pools that are variable in their content. This means that PS II RCs contain at least two additional Chls as compared to purple bacterial RCs.[17]

From its isolation the primary processes in the D1−D2 complex have attracted much attention, and a range of papers reporting ultrafast studies has been published. The first report of an ultrafast transient absorption measurement on the isolated D1−D2 complex suggested that the intrinsic charge separation rate should be 1/(2.8 ps),[18,19] i.e., in very good agreement with an early extrapolation by Schatz et al.[20,21] based on data from intact PS II particles. Roelofs et al., studying the primary events by picosecond fluorescence on an original Satoh preparation [the Chl content of that preparation might have been somewhat lower than the typical stabilized RC preparations used more recently] reported a dominant 1−7 ps charge separation component in the kinetics[22] and in addition also a slow energy transfer in the 20−30 ps region.[22,23] Very similar results were reported by us later on a now typical "6 Chl prep" which is now standard in most laboratories.[23,24] In addition the later measurements, carried out with selective P680 excitation,[24] revealed a 3 ± 1 ps main component which was assigned to the effective charge separation process, while the slow ca. 20 ps component showed a more red-shifted spectrum, identifying it clearly as an energy transfer component from some long-wave Chl. Upon selective excitation of blue pigments (around 650 nm) an additional energy transfer component of about 5 ps (this time is probably mixed with the ≈3 ps charge separation time) and also the 20−30 ps component were found. In low-temperature fluorescence measurements even more pronounced slow energy transfer components were detected.[22,23] In addition to these components a range of much slower components was detected both at room temperature and at low temperatures, ranging up to 50 ns, which were assigned mainly to radical pair recombination.[22,23] From these data Holzwarth and co-workers[24] concluded that (i) the fastest effective charge separation component in the D1−D2 RC should be approximately 3 ps, possibly with some small admixture of slower charge separation lifetimes, (ii) that a 20 ps and also an approximately 5 ps (upon blue excitation) component represented slow energy transfer times from more external Chls, and (iii) that the $Pheo^-$ formation observed with a rate constant of ca. 20 ps[25] was actually limited by the slow energy transfer from external Chls to the RC core. This interpretation was essentially supported by transient absorption measurement by Schelvis et al.[26] It was also in general agreement—as far as the comparison is justified—with previous hole burning data on the D1−D2 complex by Small et al.[27,28] This interpretation was, however, in marked contrast to the interpretation of femtosecond transient absorption data by the group of Klug and co-workers as presented in a series of papers (see, e.g., refs 25, 29, and 30). On the basis of the most extensive and detailed transient absorption studies available at that time, those authors interpreted their data in quite a different way: They (i) assigned a 21 ps component to "...reflect the effective charge separation process, not limited by an energy transfer component..." and (ii) claimed that our conclusions drawn from fluorescence data[29] "were not consistent with (their) femtosecond absorption data...". It is important to note that this different interpretation arose despite the fact that the lifetimes found in their transient absorption data on the one hand[25,29,30] and in our fluorescence experiments on the other hand[22−24] were in fact quite similar. In essence, the different assignment and interpretation of the London group was largely based on their measurement of the appearance kinetics of $Pheo^-$ at 543 nm,[25] which seems to suggest a ≈21 ps rise for $Pheo^-$ if one interprets the absorption change around 545 nm as being mainly due to Pheo.

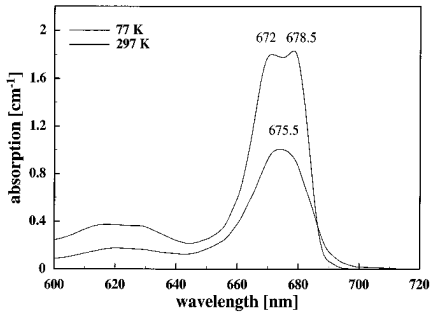

Figure 1. Absorption spectra at (A, bottom) room temperature and (B, top) 77 K of a typical D1−D2 RC sample used in these measurements. For low-temperature absorption the sample was diluted with glycerol/buffer to a final concentration of 60% (v/v) glycerol.

This fundamentally controversial interpretation of the primary processes in the D1−D2 RC has not been resolved so far. One of the main reasons for the present highly controversial discussion is the fact that it had not been possible so far for any of the research groups working in this field to present a detailed kinetic model which would in a reasonable way explain the observed kinetics in either transient absorption or fluorescence. It is clear that without such a kinetic model, which must also explain the spectra of the participating species in a reasonable way, a reliable interpretation of the data is not possible, however. Furthermore in view of the extremely complex kinetics of the primary processes in the D1−D2 complex it is highly desirable to use several different and mutually complementary techniques to study these processes. We have thus started a program to study both fluorescence and transient absorption kinetics under similar conditions in order to hopefully arrive at a fully consistent interpretation of those data. One of the essential aspects of these studies will be the use of a range of different excitation wavelengths. We present here the first part of an extensive fluorescence lifetime study carried out at a large number of different excitation/emission wavelength pairs. The data have been analyzed by global analysis methods, and furthermore a minimal kinetic scheme has been worked out on the basis of kinetic target modeling that will allow us to gain some basic insight into the excited state kinetics of the D1−D2 RC complex.

Materials and Methods

The D1−D2−cyt-b559 RCs used in this work have been isolated from spinach using the van Leeuwen method.[31] The RCs were shock frozen at 77 K until use. The Chl content of the RC preparations used in this work ranged between 6.3 and 6.6 Chl/2 Pheo,[10] as determined by HPLC. Typical room temperature and 77 K absorption spectra are shown in Figure 1.

Picosecond fluorescence has been measured by the single-photon counting method using the apparatus described previously[23,32] which allows a time resolution of about 2 ps.[33,34] Data analysis has been performed using both global lifetime (of data sets with different emission but the same excitation wavelength) and combined global lifetime (of data sets comprizing a range of different excitation and emission wavelengths) methods[23,32,35] and global target analysis methods as described previously.[34,35] For several of the critical short lifetimes an exhaustive error analysis has been carried out by calculating the corresponding section of the χ^2 surface. The relevant data are plotted as global

χ^2 vs the respective lifetime parameter. The equations used in fitting the kinetic models are given in the Appendix. The method has been described previously in detail.[32]

For measurement typically 15 ml of sample contained in a cooled reservoir in the dark was cycled by a peristaltic pump (10 mL/min) through a thermostated measurement cuvette of dimensions 1.5 × 1.5 × 1.5 mm^3. The OD was 0.8/cm at 675 nm. The buffer was 50 mM Tris-HCl, 150 mM $MgSO_4$, and 0.1% dodecylmaltoside at pH 6.5 and contained glucose/glucose oxidase and catalase for maintaining anaerobic conditions. The sample was changed regularly during the measurement process, which took typically 5−8 h for a full decay-associated emission spectrum at one excitation wavelength. No change in the kinetics nor in the stationary emission spectrum was noticed during the time within which one sample was used. In view of the complexity of the expected kinetics we accumulated data to a high *S*/*N* ratio by accumulating typically 20 000−50 000 counts in the peak channel. Data recorded with a resolution of 2 ps were analyzed over a maximal time range of 2 ns [from the same sample measurements with lower time resolution and measuring windows up to 80 ns were recorded under otherwise identical conditions; these data will be used later for a full analysis of the radical pair kinetics]. The spectral resolution was 4 nm in emission and measurements were taken every 5−10 nm. The excitation intensity was very low (2−10 mW), and we estimate that considerably less than a fraction of about 10^{-8} of the RCs was excited per pulse with a repetition rate of 800 kHz.

Results

Fluorescence kinetics have been measured for six different excitation wavelengths ranging from 620 to 689 nm and detection at several wavelengths across the entire emission range. For excitation in the long-wave range of the absorption maximum emission has also been detected at wavelengths shorter than the excitation. In order to avoid scattering of light, the detection had to be at least 10 nm apart from the excitation. Under these conditions the use of the double monochromator in emission suppressed stray light sufficiently, as has been checked by a scattering solution, and any scattering artifacts can be excluded. In all cases global analysis has been performed first on data sets corresponding to a single excitation wavelength. Usually two different analysis windows, up to 400 ps (giving best resolution for the short lifetimes) and the second one up to 2 ns (providing good resolution also for the intermediate lifetime components) have been employed. For the short time range usually four lifetime components were sufficient to describe the data for a single excitation wavelength set. For good fits in the long time range typically five lifetimes were necessary for a good fit. We show in the following only the DAS of the five-component analysis, since it generally provided the best description of the data, along with the results of the exhaustive error search for the fastest component, which is the most critical one in terms of data analysis. The four-component analyses (over a time range of only 400 ps) look quite similar, except for the fact that the three longest lifetimes, usually above 100 ps, were combined into two components only. The results of all analyses are collected in Table 1.

Figure 2 shows the full DAS (Figure 2A) and the error surface (inset) for the fastest component for an excitation wavelength of 620 nm. This corresponds to an excitation where all pigments have roughly equal chance of being excited. Characteristic for this excitation wavelength is the large negative amplitude of the fastest component, which has a lifetime of about 9 ps. The second fastest component has a lifetime of about 26 ps and has all positive amplitude. The three longest lifetimes have similar

TABLE 1: Results of Global Five-Component Analyses over a Time Window of 2 ns for the Different Excitation Wavelengths[a]

λ_{exc}, nm	τ_1, ps	τ_2, ps	τ_3, ps	τ_4, ps	τ_5, ps	τ_6,[b] ps
620		9	26	113	600	4200
650		5	31	137	880	6800
660		6	20	67	330	4300
671		5	19	60	290	4500
686	3		18	63	220	2690
689	3		25	97	420	4400
combined five-component	3[c]	6	18	92		2000
combined six-component	3[c]	6[c]	15	53	240	3400

[a] The fastest component is separated into two groups in order to indicate the two significantly different lifetime ranges found for this component for the various excitations. Errors in lifetimes are ±1 ps or ±5%, whichever is larger. [b] This lifetime is not determined well in the time windows used for the analysis. [c] Lifetimes that were fixed in the analysis.

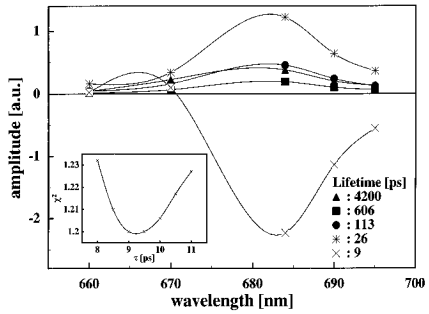

Figure 2. Decay-associated emission spectra (DAS) as obtained from five-component global analysis (over a time scale of 2 ns) of the data set with excitation wavelength 620 nm. Inset: χ^2 surface for the fastest component as obtained by exhaustive error analysis in global mode. Note for Figures 2−7: The four-component analyses (carried out over a time range of only 400 ps) look quite similar, except for the fact that the three longest lifetimes, usually above 100 ps, were combined into two components only.

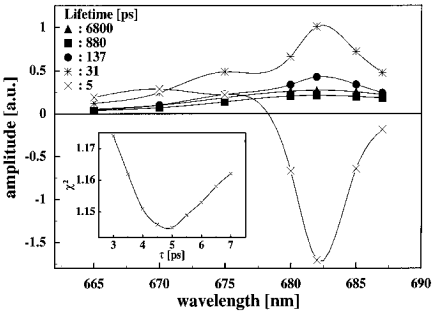

Figure 3. DAS for excitation wavelength 650 nm and χ^2 surface (inset) for the fastest component. For further explanations see caption to Figure 2.

spectra. The plot of the error surface (inset) shows clearly that the 9 ps lifetime is quite well-defined. Figure 3 shows the corresponding data for an excitation wavelength of 650 nm, i.e., at the short-wave edge of the Q_y absorption band. Again there is a fast component with a large negative amplitude. Its lifetime is significantly shorter (ca. 5 ps), however, than for 620 nm excitation, as can be seen also from the plot of the error surface (inset). The second fastest lifetime is about 30 ps. The situation is quite similar for λ_{exc} = 660 nm (Figure 4). The shortest lifetime of 6 ps is now less well-defined (inset) with an error surface somewhat more flat toward longer lifetimes. The second fastest component is 20 ps, i.e., significantly shorter than for 650 nm excitation. A very similar set of lifetimes is obtained for λ_{exc} = 671 nm (Figure 5). However, the DAS of the shortest lived component (5 ps) has its zero-crossing wavelength now very much shifted to the red, i.e., to about 685 nm. Below that

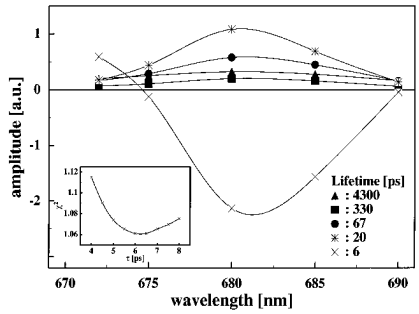

Figure 4. DAS for excitation wavelength 660 nm and χ^2 surface (inset) for the fastest component. For further explanations see caption to Figure 2.

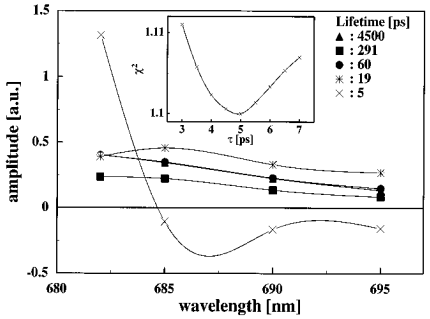

Figure 5. DAS for excitation wavelength 671 nm and χ^2 surface (inset) for the fastest component. For further explanations see caption to Figure 2.

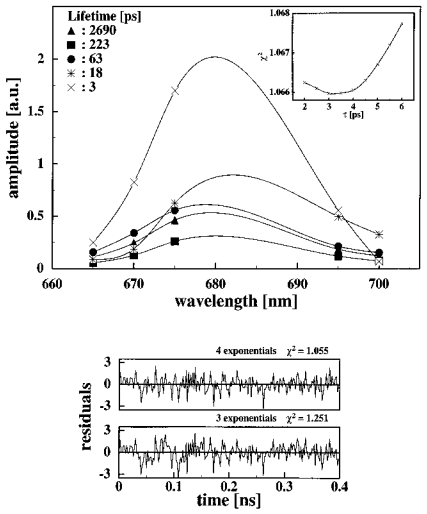

Figure 6. (A, top) DAS for excitation wavelength 686 nm and χ^2 surface (inset) for the fastest component. (B, bottom) Comparison of the residuals plots (675 nm) with and without the 3 ps component. For further explanations see caption to Figure 2.

wavelength the amplitude is strongly positive. The error analysis for the fast component shows a well-defined minimum at 5 ps (inset). The situation changes entirely upon shifting the excitation wavelength to 686 nm (Figure 6). Now all components are positive in the detection wavelength range (up to 700 nm). The fastest lifetime is now about 3−4 ps and has a dominant and all-positive amplitude. The error analysis of the shortest component shows clearly that the lifetime must be significantly below 5 ps (inset), close to the shortest one that had been found for the shorter excitation wavelengths. Figure 6B compares the residual plots for analyses taking into account or ignoring the ≈3 ps component. Finally Figure 7 shows the DAS for an excitation wavelength of 689 nm, i.e., at the extreme red edge of the absorption spectrum. Again all components are positive in amplitude, and the shortest lifetime is about 3 ps. Note that the 3 ps component has ≥50% of the total

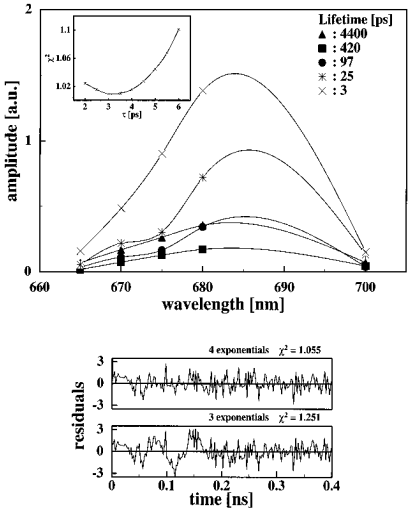

Figure 7. (A, top) DAS for excitation wavelength 689 nm and χ^2 surface (inset) for the fastest component. (B, bottom) Comparison of the residuals plots (680 nm) with and without the 3 ps component. For further explanations see caption to Figure 2.

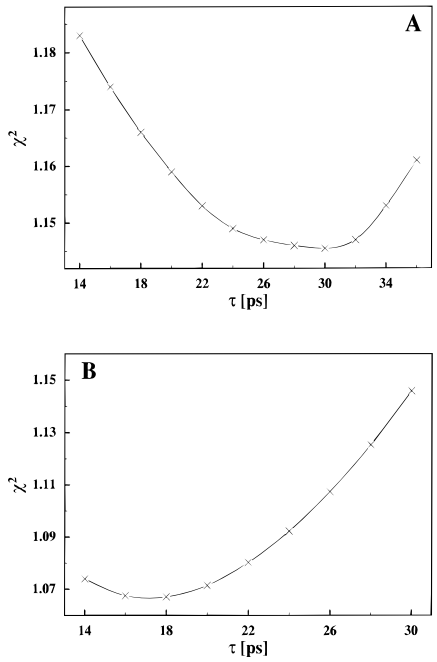

Figure 8. χ^2 surfaces for the second fastest component for excitation wavelengths of 650 (A) and 686 nm (B).

amplitude around 680 nm, as was also the case in Figure 6. Again the residuals plots (Figure 7B) show the necessity of the 3 ps component.

An excitation wavelength of 680 nm, although probably most selective for P680 excitation, was found not to be very informative. This is due to the fact that under such excitation conditions the available detection range (due to scattering near the excitation wavelength) would have been limited to below 670 nm and above 690 nm only, i.e., to wavelength ranges which contribute the least amount of information on the energy transfer processes.

Figure 8 shows two error surfaces for the second fastest component for 650 nm (Figure 8A) and 686 nm (Figure 8B) excitation, respectively. The error surfaces clearly show that these lifetimes are significantly different. From the DAS one notices furthermore that in particular the DAS of the ca. 18 ps component is significantly red-shifted against all the other components (c.f. Figure 5). We note that this component is

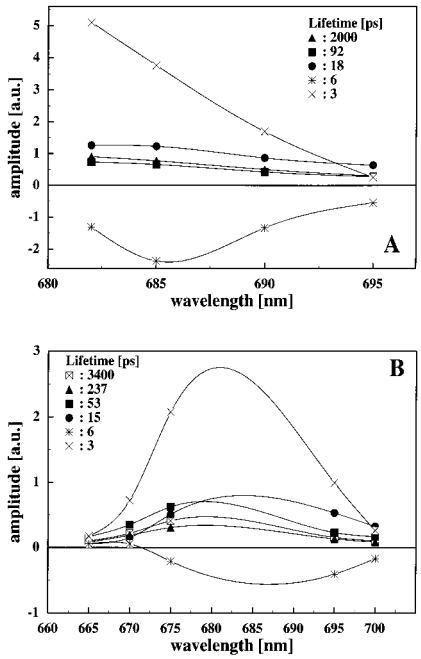

Figure 9. (A) DAS from a combined global analysis of all excitation wavelengths over 400 ps with five components. Data are shown for excitation of 671 nm only. The decays for some excitation wavelengths are not described optimally by such a five-component analysis. (B) DAS from a combined global analysis of all excitation wavelengths with six components. Data are shown for excitation of 686 nm only. The two fastest lifetimes were fixed in this analysis (see text). The whole data set is described well in this analysis.

essentially missing in samples which are very low in the so-called "red Chl".[56]

Combined Global Analysis. It follows from Table 1 that in particular the fastest lifetime (separated already into two ranges in Table 1) shows a large systematic dependence on excitation wavelength, falling into two ranges of about 3 and 5−9 ps, respectively. The same is true for lifetime τ_4 which ranges from about 50 to 140 ps (see Table 1). Thus, a five-component analysis will not be sufficient to describe the complete data set for all excitation wavelengths simultaneously over a time range of 2 ns. Such combined global analyses were performed, combining the whole data set including all excitation wavelengths. In these analyses either the fitting window had to be reduced (from the 2 ns windows used in the separate global analyses described above) and/or the number of components had to be increased in order to achieve a good fit for all of the excitation wavelengths simultaneously. Parts A and B of Figure 9 show two examples from combined global analyses with five and six components, respectively, over a time window of 400 ps each. The predominant feature of these combined analyses is that the fastest component splits into two components (3 and 6 ps), as was already expected on the basis of the excitation wavelength dependence of the fastest lifetime. The third component is in the range of 15−18 ps. From these analyses it follows that the fastest (3 ps) component has positive amplitude over the whole excitation and detection wavelength range, while the second component (ca. 6 ps) shows positive/negative features for nearly all excitation wavelengths. Furthermore it is found that the third component (15−18 ps) has a significantly red-shifted DAS as compared to all of the other components. All components above ca. 50 ps have very similar DAS. The results of these combined analyses are also collected in Table 1. It is important to note, however, that for the six-component analysis which leads to a perfect description of the whole excitation/emission data surface, it was not possible to have all of the lifetimes free-running. Thus, the fastest component (3 ps) and sometimes also the second fastest component were fixed in the analysis around the values that were found optimal for the individual global analyses. Several combinations of these fixed lifetimes were then tried until the optimal combination that resulted in the best fit was found (shown in Table 1 and Figure 9B). On the one hand the data, as judged on the basis of residual plots, indicate that six components are indeed required for a good description of the whole data surface on a 400 ps time range. On the other hand, as a consequence of this large number of components, we have to accept an increased uncertainty in the value of the fastest lifetimes. However, it should be noted that all of the DAS obtained in the six-component analysis look quite reasonable and do not show any oscillations nor a compensatory behavior of two components, as is often observed for example when using too many components in a fit. Again the combined global analysis confirms that the 3 ps component is the dominant amplitude ($\geq$50%) component in the fluorescence decays for red excitation wavelengths where the RC core is preferentially excited.

With increasing complexity of the system the analysis of the fluorescence decay kinetics within a discrete sum-of-exponentials model may become questionable. Whether this is actually the case can be tested by applying data analysis procedures that allow for distributions in lifetimes.[36] Thus, we carried out a lifetime distribution analysis on the measured fluorescence kinetics. The result of these analyses (not shown) is that the discrete character of the fluorescence kinetics, as obtained from the discrete global analysis by sums of exponentials, is supported. Thus, the maxima of the distribution bands are located at the same lifetimes as in the discrete analysis, and the narrow relative width of the distributions obtained does not suggest the presence of any substantial rate distributions. Of course this statement applies to the limits set by the achieved *S*/*N* ratio in the data, which is quite high however.

Discussion

The excited state kinetics of D1−D2 RCs is found to be extremely complex. From the individual and combined global analyses it follows that a minimum of six components is necessary to describe the whole excitation/emission data surface over a time range of $\geq$400 ps. The fastest component of 3 ps is the dominant component for all excitation wavelengths in the combined global analysis. Its amplitude is positive for all detection wavelengths up to 700 nm with an emission maximum in the range of 680−685 nm. The second component of about 6 ps shows either negative amplitude over the whole emission range (Figure 9) for some excitation wavelengths or a positive/negative amplitude feature for other excitation wavelengths (c.f. Figure 3A). This component can thus clearly be assigned to an energy transfer origin. The 18 ps component is red-shifted in its DAS as compared to all of the other DAS. It is thus likely that it also arises due to energy transfer. Interestingly for short-wave excitation (650−660 nm range in particular) this lifetime is closer to 30 ps and under such conditions it is not red-shifted but more blue-shifted as compared to the DAS of the 3 ps component. The longer lived components show DAS that are very similar to each other and also similar to the DAS of the fastest component. This suggests that the excited state-(s) giving rise to these components may be also similar or even identical.

The following conclusions can be drawn from these observations: The data are consistent with the hypothesis that the 3 ps component is the dominant charge separation component. This follows mainly from the fact that it is positive across the whole measured detection range (at least up to 700 nm) and that its

DAS is the dominant amplitude component for all excitation wavelengths. Furthermore its spectrum is quite similar to that of the long-lived components which most probably arise from charge recombination of the radical pair, known to live for about 50 ns at room temperature, and are thus expected to have the same or at least a very similar excited state origin. It is important to note, however, that this hypothetical assignment of the 3 ps component cannot be finally proven on the basis of the global DAS alone. In view of the very complex kinetics such a proof rather requires a detailed kinetic modeling which is presented below. Further conclusions that can be drawn from the global lifetime data concern the presence of two and most probably three different Chl pigment pools that transfer their energy relatively slowly to P680. These energy transfers should be associated with the lifetime components of about 6 and 18 ps, which show quite distinct DAS, and probably also with a lifetime component of about 30 ps, which for short excitation wavelengths shows a blue-shifted DAS. Again these assignments need to be checked and can only be finally proven on the basis of a detailed kinetic modeling.

Kinetic Modeling. In the following we will perform kinetic modeling on the originally measured lifetime data (not on the DAS results of Figures 2−7 which are already derived data). The final long-term aim will be to arrive at a single kinetic scheme that (i) is suitable to describe the fluorescence kinetic data for all excitation wavelengths simultaneously, (ii) that is unique, and furthermore (iii) that is consistent with other (structural and kinetic) data and knowledge on the D1−D2 complex.

In view of the complexity of the system this is quite a challenging task, and we consider it unlikely that it can be achieved in a single step. For this reason we will proceed in a stepwise manner. In the first step we will try to develop minimal kinetic models that describe the kinetic data well at least for one excitation wavelength. The rationale behind this approach is that, despite the fact that we are dealing with a connected kinetic system of high complexity, it will be possible for certain specific excitation conditions to ignore some (more slowly coupled) parts of the system in the kinetic model. In a first order approach this might give some further insight into the system that should help us to eventually arrive at an undoubtedly more complex unified kinetic scheme. Note that we limit ourselves here entirely to such models which can be described by first order rate equations; i.e., we do not test any models which would contain distributed rate constants (see also comment above).

Basic Assumptions of the Models. It is well-known from transient absorption measurements that there exist fast (≤500 fs) kinetic components which connect various chromophores in the RC core with P680 by ultrafast energy transfer steps.[24,35,37] We can thus assume that prior to charge separation there occurs subpicosecond equilibration within this RC core. We do not make any assumptions, however, with regard to the size and/or composition of this core except that P680 should be part of it and that this core comprizes all of the chromophores that are coupled to P680 on a subpicosecond time scale. Furthermore we will assume in our kinetic models the presence of one or more radical pairs which are in equilibrium with the excited state of P680 (viz., the excited RC core) via a charge separation/charge recombination equilibrium. We will, however, only perform a minimal description of the radical pair kinetics in this paper, as far as it is necessary to get a correct description of the energy transfer and primary charge separation kinetics, since the full complexity of the radical pair (RP) kinetics will be addressed in detail in a separate paper. Charge recombination luminescence has been demonstrated by several groups convincingly for the isolated D1−D2 complex and the presence of several long-lived components suggests the presence of several RPs.[22,23,38−40] Furthermore such an equilibrium is well-established to exist in intact PS II particles[21,32,41] and also in isolated bacterial RCs.[33,42] In addition we will allow for two (see above) or three additional pigment pools which transfer their energy on a relatively slow time scale of a few picoseconds or longer to the RC core. We furthermore assume a homogeneous pigment composition for all of the D1−D2 particles in the sample [we have proposed previously that the pigment content of isolated D1−D2 complexes is not stoichiometric;[10] this implies that an ensemble of D1−D2 complexes contains particles with different pigment contents; this will be ignored in our present analysis]. No further assumptions will be made for the kinetic modeling, except that we are looking for the simplest kinetic model(s) that are suitable to explain the data. These models comprize the minimally required number of external Chls besides the RC core and a single radical pair. Most importantly, we do not make any a priori assumptions about the rate constant of charge separation nor about which of the observed lifetime components is associated with charge separation. From this kinetic modeling we should in principle be able to obtain the (effective) rate constants, the species-associated emission spectra (SAES) (i.e. the emission spectra of the excited or pseudoexcited states in the model) and with some restrictions, the relative excitation probabilities for the corresponding ground states (excitation vector).[35] The method used for modeling the data is global target analysis on the original measured data sets using a Levenberg−Marquardt optimization procedure.[43] The rate constants of the model and the SAES are optimized simultaneously. Full details of the procedure are given in ref 35.

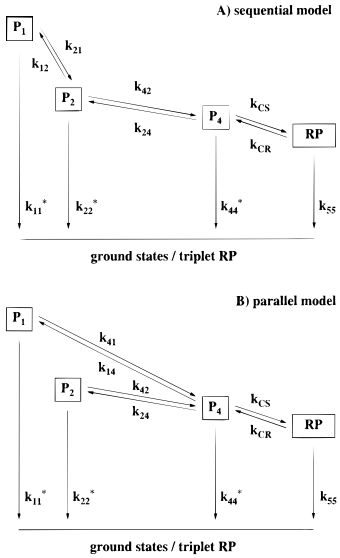

Figure 10. Kinetic schemes that describe the data for the short excitation wavelength range well. P_i refers to the excited Chl. P_4 corresponds to the RC core. RP1 denotes primary radical pair, and RP2, the secondary radical pair.

Minimal Kinetic Models. For the excitation wavelengths of 620−660 nm the simplest kinetic models that describe the data reasonably well in accordance with the basic model assumptions described above consist of the RC core (including P680), a radical pair, and two additional pigment pools with relatively slow energy transfer to the RC core. Within this model two kinetic schemes which describe the data about equally well are possible: the sequential scheme (Figure 10A) and the parallel scheme (Figure 10B). The resulting SAS for an excitation wavelength of 650 nm are shown in Figure 11. [The shape and spectral maxima of the SAS are essentially the

TABLE 2: Rate Constants from Kinetic Modeling of Data from Individual Excitation Wavelengths by Global Target Analysis[a]

conditions	k_{21}	k_{12}	k_{41}	k_{14}	k_{43}	k_{34}	k_{42}	k_{24}	k^{cs}	k^{cr}	k_{55}, k_{66}[b]	k_{65}	k_{56}
model A ≤ 650 nm	150	55					50	11	131	53	11		
model B ≤ 650 nm			185	31			45	10	121	53	20		
≥671 nm			115	9	80	30			149	73	0.03; 1.9	14	10
combined target analysis; model Figure 13A	143	46			78	30	42	10	115	65	0.03; 0.03	15	8
combined target analysis; model Figure 13B			148	47	85	33	37	6	128	58	0.03; 0.03	15	11

[a] Rate constants k_{ij} in [ns^{-1}]. The nomenclature corresponds to the kinetic schemes in Figures 10 and 12. k^{cs} refers to the (*effective*) rate constant of charge separation and k^{cr} to the rate constant of charge recombination. Errors in rate constants may be up to ±20%. [b] Recombination rates to triplet and/or ground state in six-component analysis.

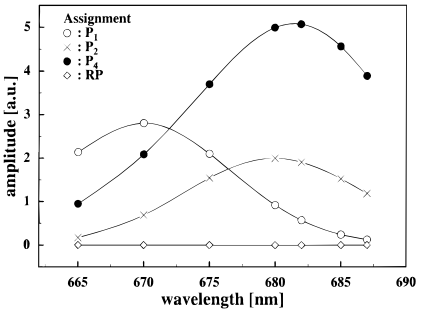

Figure 11. SAES resulting from the analysis of 650 nm excitation data using the kinetic schemes in Figure 10. (The SAES for schemes A and B in Figure 10 are very similar in shape and position.)

TABLE 3: Lifetimes τ_i (ps) Resulting from the Various Kinetic Models Based on Rate Constants Shown in Table 2

conditions	τ_1	τ_2	τ_3	τ_4	τ_5	τ_6[a]
model A ≤ 650 nm excitation	4	5	27	140		4000
model B ≤ 650 nm excitation	4	7	21	87		8500
≥671 nm excitation	4	9	13	56		1100
combined target analysis; sequential model Figure 14A	4	5	13	30	64	3600
combined target analysis; parallel model Figure 14B	3	8	12	26	52	3500

[a] This lifetime is not determined well in the used fitting windows of 400 ps.

same for both models. However, the relative amplitudes of $SAES_1$ and $SAES_2$ are somewhat different for the two models. Note that the number notation for the different species will be uniform throughout this paper. For example, in the two models applied here species 3, which will be required for longer excitation wavelengths, has been ignored.] The rate constants for the two models are shown in Table 2 and the resulting lifetimes in Table 3. Model 10B (parallel scheme) results in lifetimes that are in slightly better agreement with those from the combined global lifetime analysis. However, distinction between these two models is not easily possible. There are some common features of the models: Effective charge separation (from pigment pool 4, which contains P680) and charge recombination, respectively, occur with approximately the same rate constants in both models, and the energy transfer from the pigment pool 1 is very fast (150 and 185 ns^{-1}, respectively). This assignment is clearly possible, since pigment pool 4 is the one which is connected with the nonfluorescent (i.e., SAES = 0) radical pair state. In both models the main component of charge separation is associated with the ≈3−4 ps component [note that the 3−4 ps component which is dominant in primary charge separation is an *effective* lifetime which is determined not only by the charge separation rate constants but also by the fast energy transfer steps], if the RC core (pigment pool 4) is preferentially excited (between 70 and 80%), which is the case (to different extents) for all excitation wavelengths used in this work. Within a more simplified model with only one additional pigment pool it was not possible to describe the experimental data adequately.

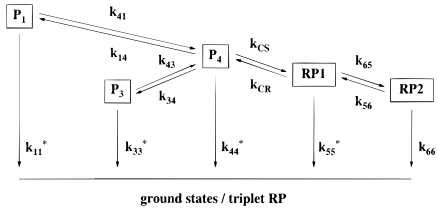

Figure 12. Kinetic scheme that describes the data for the long excitation wavelength range well. P_i refers to the excited pigment pools. P_4 corresponds to the RC core. The rate constants denoted by an asterisk have been fixed in the analysis to values of 0.3 and 0.03 ns^{-1}, respectively (see text). RP1 denotes the primary radical pair, and RP2, secondary radical pair.

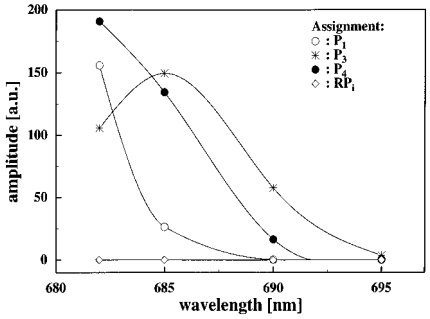

Figure 13. SAES for long excitation wavelengths resulting from the analysis using the kinetic scheme shown in Figure 12.

For longer excitation wavelengths (671 nm and above) the minimal kinetic model involves also the RC core, two additional pigment pools and at least one radical pair (taking into account two sequentially created radical pairs gives a much better description for the time range up to 2 ns). The corresponding kinetic scheme of the model is shown in Figure 12 and the resulting SAES for an excitation wavelength of 671 nm in Figure 13. In the scheme and the SAES of Figures 12 and 13 one of the two additional pigment pools is numbered 3, since clearly its SAES is substantially red-shifted as compared to the other SAES and does not agree with that of pigment pool 2 found in the analysis for shorter excitation wavelengths (see above). Correspondingly pigment pool 2 has been ignored from the minimal scheme in Figure 12. Unlike the situation shown in Figure 10, for the long excitation wavelengths the data are only consistent with a kinetic model where the two additional pools (i.e., pools 1 and 3) are not directly connected with each other. Thus, only one kinetic scheme is possible. Again pigment pool 1 has a very fast energy transfer to the RC core, and charge separation occurs with a rate constant that is only slightly higher than for the models in Figure 10 (suitable for short excitation wavelengths). The inclusion of a second radical pair improves the fitting substantially. [The question of radical pair kinetics is a different subject. In this work it is not our aim to analyze or assign the radical pair kinetics in detail. The sequentially connected two radical pairs (both have SAES = 0, i.e., are nonfluorescent) in this model are thus considered here simply as a suitable mathematical description of the observed kinetics. We do not necessarily imply at this stage that two different

radical pairs are connected in this way.] The fastest lifetime of about 4 ps is again associated with the predominant component of charge separation. The pigment pool 3 has a SAES whose maximum is red-shifted with respect to that of pigment pool 4 (corresponding to the RC core). It is thus likely that pigment pool 3 corresponds at least partly to the "red Chl" found in low-temperature fluorescence spectroscopy[44] and also in hole-burning spectroscopy.[27] This red Chl pool is connected with the RC core by a relatively slow energy transfer which gives rise to a lifetime of about 13 ps in the first order kinetic model.

For all of the minimal models that describe the kinetics reasonably well for a limited wavelength range (Figures 10 and 12) the effective charge separation has an optimal rate constant in the relatively narrow range of 100−150 ns^{-1}. It is not possible to use substantially slower charge separation rates since this leads to drastically decreased fit quality. For example a charge separation rate constant fixed to 50 ns^{-1}, i.e., the fastest one that might be compatible with a suggested effective charge separation lifetime of about 21 ps,[30] would lead to a very poor fit that is totally inconsistent with the data. Taking into account the fact that the models tested so far are only minimal models and each of them clearly does not describe the entire data surface, we should be prepared to accept a relatively large systematic error for several of the rate constants determined here, including k^{cs}. Nevertheless from all of the individual kinetic modeling runs we can conclude that if we set the error limits in a very conservative fashion, the effective rate constant k^{cs} for charge separation (from the equilibrated core) must be larger than 90 ns^{-1} and most probably smaller than 160 ns^{-1}. In all cases studied this implies that the apparent charge separation kinetics is associated primarily with the fastest lifetime of about 3−4 ps found in the individual target analyses. This is a very stable feature of all of the models presented above (and the more complex ones presented below) indpendent of any other details of the models.

Combined Target Analysis. In the following we make an attempt to develop a uniform model that should be suitable to describe the kinetics for all excitation/emission wavelength pairs simultaneously. From the results of the simpler kinetic models presented above it follows that such a unified model will comprize the RC core, three additional pigment pools (corresponding to pools 1, 2, and 3 from the first order kinetic models) and two or even three radical pair states. Such a model is quite complex. Its merits and present limitations will be discussed below in detail. From the models in Figures 10 and 12 it follows that, at least formally, two kinetic schemes should be suitable to describe the kinetics over the entire excitation/emission data surface. These two schemes are shown in parts A (sequential model) and B (parallel model) of Figure 14. The corresponding optimized rate constants for these models are given in Table 2 and the resulting lifetimes in Table 3. The results of these analyses are in reasonable agreement with the simpler first order models. The rate constants for charge separation are in the range of 115−130 ns^{-1}, i.e., in good agreement with the corresponding rate constants in the simpler models. This again has the consequence that the fastest lifetime of 3−4 ps describes the dominant part of the charge separation. Although the kinetic systems are strongly coupled and thus the kinetic constants (lifetimes) cannot be interpreted in a simple way, to a first approximation the lifetimes of 5−8 ps are mostly due to the decay of/to pigment pool 1 and the lifetime of 12−13 ps corresponds mainly to the kinetics of pigment pool 3, while the lifetime of 26−30 ps corresponds to the lifetime of pigment pool 2. The lifetime of ca. 50 ps corresponds to a relaxation process between radical pairs.

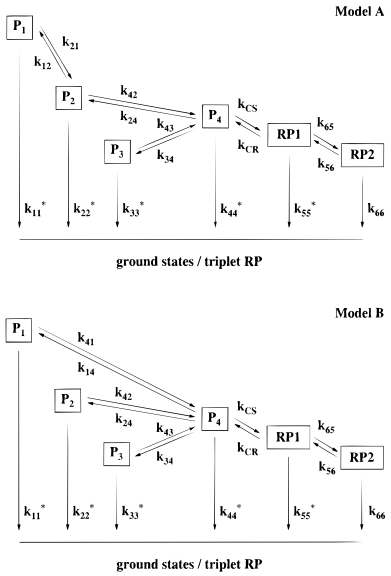

Figure 14. Kinetic schemes for a unified kinetic model describing the whole kinetic fluorescence data surface: (A) sequential model; (B) parallel model. RP1 denotes the primary radical pair, and RP2, secondary radical pair.

We do not show here the resulting SAES for these models for several reasons: The prima facie reason is that, unlike the SAES for the models in Figures 11 and 13, the SAES for the combined models are fairly "noisy", which is a sign of the relatively large uncertainties of up to ±30% in the relative amplitudes and thus in the exact shapes of the spectra if no restrictions based on other experimental data are used in the fits. Furthermore, several of the SAES are highly correlated. This means that a change in one spectrum can be compensated for to a large part by a change in another spectrum. A further problem is the precise definition of the absorption probabilities (excitation vector). As a consequence it is clear that further improvements in the analysis are necessary before final reliable spectra can be presented. However, the analysis shows also that the correlations in the rate constants and thus in the corresponding errors are much smaller than for the spectra. We estimate that most rate constants may have an error of up to ±20%. Notwithstanding later improvement in precision, this sufficiently justifies that the set of rate constants is presented here as a first result of a global fitting procedure attempting to produce a consistent model that describes the whole fluorescence data surface. The fit quality for both combined models (Figures 14A,B) is quite similar (χ^2-values of 1.12 and 1.19, respectively), and on the basis of these fits we can at present not decide between these two models. We have a slight preference for model 14B for the following reason: In our spectral analysis pigments P_1 and P_2 belong to the Chls at the periphery of the RC core, which are both present to nearly a full equivalent of a Chl; i.e., these Chls are present in all preparations.[10] It has been proposed that the binding sites for these external Chls should be the two His residues in position 118 in helix II of the D1 and D2 proteins which are not present in the sequence of bacterial RCs.[45] If this assumption is correct, then these two peripheral Chls should have a relatively large distance to each other[46,47] (probably larger than about 30 Å). This would not allow relatively fast energy transfer among them, as would be required in model 14A but not in model 14B. We will nevertheless in the future continue to test both models for their compatibility with the data, in particular also with femtosecond transient absorption.

"Intrinsic" Charge Separation Rate Constant. The *effective* charge separation rates obtained in the various kinds of models presented in this paper range between 100 and 150 ns^{-1}.

The *intrinsic* charge separation rate must be several-fold higher than these values since the intrinsic and the effective rate constant are connected by the following equation:[21]

$$k_{\text{int}}^{\text{cs}} = k_{\text{eff}}^{\text{cs}} \frac{1}{P} \tag{1}$$

where P is the probability that the excitation is actually located on P680. Since the RC core contains several chromophores which are nearly isoenergetic with P680 and there occurs a very rapid (subpicosecond) equilibrium of excited states in the RC core, we estimate that P could range from about 0.25 to 0.5, depending on the spectral model one accepts for the RC core.[10] This means that the intrinsic rate constant $k_{\text{int}}^{\text{cs}}$ should have a minimal value of 200 ns^{-1} and a maximal value of about 500 ns^{-1}. From our modeling an effective rate $k_{\text{eff}}^{\text{cs}} \approx 120\ \text{ns}^{-1}$ is the most likely one, and in our spectral model[10] the occupancy factor P is calculated to be about 0.3 which then results in an intrinsic charge separation rate of about 360 ns^{-1} or a 2.7 ps intrinsic lifetime. We note that this is in excellent agreement with our earlier extrapolation for this rate in intact PS II particles.[21] If one were to take the 21 ps lifetime as the *apparent* charge separation lifetime as proposed by Klug and co-workers,[25,30] in the simplest kinetic model the maximal effective charge separation rate would be about 50 ns^{-1} (taking the inverse of the effective charge separation lifetime), and it would be even substantially lower in more realistic models taking into account the energy transfers to the external Chls [note that in the models presented here the 3−4 ps effective charge separation lifetime corresponds to an effective charge separation rate constant of ≈120 ns^{-1}].

$$QY^{\text{cs}} = \frac{k_{\text{app}}^{\text{cs}}}{\sum k_i}$$

$$k_{\text{app}}^{\text{cs}} = 1/\tau_{\text{int}} N_{\text{eff}} \tag{2}$$

Performing a similar calculation as above this would then result in an intrinsic charge separation rate of not more than 150 ns^{-1}, i.e., by a factor of at least 2−3 lower than that found here. Such a low value is clearly inconsistent with our data on isolated D1−D2. It is also important to note however that such a low value would also be in conflict with a high yield of charge separation in the native PS II complex. This can be estimated easily based on an effective antenna size of about 140 of the native PS II complex (total antenna size about 225 Chls a + b in BBY particles; decomposition of the absorption spectrum as described in ref 48), taking the relationships given in ref 21 into account (see eq 2); (QY^{cs} is the yield of primary charge separation and N_{eff} is the effective antenna size, i.e., the effective number of Chls isoenergetic with the RC primary donor, and $\sum k_i$ is the sum of the rate constants of the processes deactivating the excited state) and taking the data from ref 32. Thus, an intrinsic charge separation lifetime of 2.6 ps allows for a ≈90% yield, in good agreement with measured data for intact systems. In contrast the yield would drop to about 68% only for an intrinsic charge separation lifetime of about 10 ps. Such a low yield would be clearly inconsistent with an efficient photosystem II function. If that slow charge separation lifetime were indeed present in isolated D1−D2 complexes, as suggested by Klug and co-workers,[30] one would have to conclude that the isolated D1−D2 complexes are not representative of intact RCs and were damaged in their function substantially as a consequence of the isolation process. This is however not the case, as is demonstrated in this study.

Conclusions

Extensive kinetic modeling on a very large data set of ultrafast kinetics of the primary processes in the D1−D2 complex has been performed for the first time. Previous measurements carried out either in fluorescence or transient absorption have never been tested by kinetic modeling which is probably one of the main reasons for the continuing dispute about the rate of the primary charge separation. All of this kinetic modeling, whether performed on minimal models and data from single excitation wavelengths or on the more complex models, incorporating the full data set of all excitation/emission wavelength pairs, have consistently shown that any effective charge separation rate of less than 80 ns^{-1} is entirely inconsistent with the data. Despite the fact that we can at present not propose a unique kinetic model we note that the various alternatives only differ in the energy transfer properties and the arrangement of the external Chls relative to the RC core, but they do not differ principally in the primary charge separation rate. Despite the difficulties in unraveling the extremely complex excited state kinetics of the isolated D1−D2 complex it is gratifying to see that the assignment of the experimental ≈3 ps component to effective primary charge separation on the one hand and the assignment of the ≈10−20 ps components to energy transfer on the other hand is in fact a very robust feature common to all of the different models of varying complexity. This makes us very confident that our assignment is correct and that we can definitely exclude the contrasting assignment by Klug and co-workers.[30] We also note that our assignment is well-supported by the results from our low-intensity femtosecond transient absorption experiments.[49]

A general feature of all of the models, again independent of any further details, is the relatively high charge recombination rate in the range of 50−80 ns^{-1} from the first radical pair into the excited state. This must be interpreted as indicating a relatively small loss of free energy in the primary charge separation step(s) as compared to intact photosystem II.[21,32,41] Even taking into account the several-fold higher intrinsic charge separation rate from the excited P680, a relatively small energy gap between P680* and the first RP of only ≈−40 meV results. Further understanding of this remarkable phenomenon must await a more extensive and detailed characterization of the nature of the radical pair state(s) and the relaxation steps involved.

Our analyses show that at least three spectrally and kinetically distinguishable Chls are located at the periphery of the RC core in isolated D1−D2 complexes and that these Chls exchange energy with the core relatively slowly, on the time scale of 6−30 ps. The presence of the external Chls, quite in contrast to the situation encountered in, e.g., purple bacterial RCs,[50] has a profound influence on the entire observed kinetics and leads to substantial difficulties for unraveling the effective charge separation kinetics. Evidence for these slow energy transfers has been obtained by us already earlier,[22−24,51] and the present kinetic analysis now reveals this in more detail. The ratio of the forward to backward rates of energy transfer found in the kinetic analyses and the corresponding energy difference based on a Boltzmann equilibrium is in quite good agreement with the energetic differences found in the spectral positions of the various pools (SAES maxima). This provides independent support for the validity of the concept. Furthermore the finding of three distinguishable Chl pools is also in agreement with our detailed spectral analysis which required the presence of three different additional Chl pools outside the RC core.[10]

All of our data and kinetic analyses indicate that the radical pair kinetics is quite complex, requiring the presence of several kinetically different radical pair states. In principle this is in

agreement with previous data both from our group[22,23,52] and from Klug and co-workers.[38,53] Formally the observed kinetics can best be described by a sequential radical pair relaxation kinetics as has been suggested also in RCs of purple bacteria.[54,55] However, various other models may be possible, and we have not tested here scrutinely all alternative models for the radical pair kinetics in PS II RCs which will be the subject of a subsequent paper.[57]

Acknowledgment. We thank M. Reus and U. Pieper for isolating the reaction centers. Partial financial support has been provided by the Deutsche Forschungsgemeinschaft (Sonderforschungsbereich 189, Heinrich-Heine-Universität Düsseldorf and Max-Planck-Institut für Strahlenchemie, Mülheim a.d. Ruhr) and the European Community Human Capital and Mobility Program. We also thank Prof. K. Schaffner for support of this work.

Appendix

The equations that were solved to describe the kinetics and fit the species-associated spectra and rate constants are as follows:

$$\dot{\mathbf{X}}(t) = \mathbf{T}\cdot\mathbf{X}(t) + \epsilon\cdot l(t)$$

where $\mathbf{X}(t) = (n \times 1)$ vector of concentrations of (excited state) species, $\dot{\mathbf{X}}(t)$ = time derivative of $\mathbf{X}(t)$, $\mathbf{T} = (n \times n)$ kinetic matrix describes connectivity of system, T_{ij} = rate constants k_{ij}, $T_{ii} = T_{0i} + \sum_{j=1;(j\neq i)}^{N} T_{ji}$, ϵ = vector of time zero absorbances of species, and $l(t)$ = excitation function, with

$$F(t,\lambda_i) = \sum_{j=1}^{n} \exp(\gamma_j t) \sum_{k=1}^{n} S_k(\lambda_i)(\mathbf{U}^{-1}\cdot\epsilon(\vec{\lambda}_{\mathrm{exc}}))_j\cdot\mathbf{U}_{jk}$$

where $F(t,\lambda_i)$ = the decay data as a function of wavelength and time, $\gamma_j = j$th eigenvalue of matrix kinetic matrix $\mathbf{T}$, $\mathbf{U}$ = matrix of eigenvectors of $\mathbf{T}$, n = number of (excited state) species k, and $S_k(\lambda_i)$ = species-associated emission (SAES) or difference spectrum (SADS) of kth species.

References and Notes

(1) Renger, G. *Photosynth. Res.* **1993**, *38*, 229.
(2) Nanba, O.; Satoh, K. *Proc. Natl. Acad. Sci. USA* **1987**, *84*, 109.
(3) Barber, J.; Chapman, D. J.; Telfer, A. *FEBS Lett.* **1987**, *220*, 67.
(4) Braun, P.; Greenberg, B. M.; Scherz, A. *Biochemistry* **1990**, *29*, 10376.
(5) Chapman, D. J.; Gounaris, K.; Barber, J. *Biochim. Biophys. Acta* **1988**, *933*, 423.
(6) Barber, J. *Trends Biochem. Sci.* **1987**, *12*, 321.
(7) Hansson, O.; Wydrzynski, T. *Photosynth. Res.* **1990**, *23*, 131.
(8) Trebst, A.; Depka, B.; Kipper, M. In *Current Research in Photosynthesis. I*; Baltscheffsky, M., Ed.; Kluwer Academic Publishers: Dordrecht, The Netherlands, 1990; p 217.
(9) Groot, M. L.; Peterman, E. J.; van Kan, P. J. M.; van Stokkum, I. H. M.; Dekker, J. P.; van Grondelle, R. *Biophys. J.* **1994**, *67*, 318.
(10) Konermann, L.; Holzwarth, A. R. *Biochemistry* **1996**, *35*, 829.
(11) van Kan, P. J. M.; Otte, S. C. M.; Kleinherenbrink, F. A. M.; Nieveen, M. C.; Aartsma, T. J.; van Gorkom, H. J. *Biochim. Biophys. Acta* **1990**, *1020*, 146.
(12) Otte, S. C. M.; van der Vos, R.; van Gorkom, H. J. *J. Photochem. Photobiol. B* **1992**, *15*, 5.
(13) Montoya, G.; Cases, R.; Yruela, I.; Picorel, R. *Photochem. Photobiol.* **1993**, *58*, 724.
(14) Aured, M.; Moliner, E.; Alfonso, M.; et al. *Biochim. Biophys. Acta* **1994**, *1187*, 187.
(15) Chang, H.-C.; Jankowiak, R.; Reddy, N. R. S.; et al. *J. Phys. Chem.*, in press.
(16) Eijckelhoff, C.; Dekker, J. P. *Biochem. Biophys. Acta* **1995**, *1231*, 21.
(17) Michel, H.; Deisenhofer, J. *Pure Appl. Chem.* **1988**, *60*, 953.
(18) Wasielewski, M. R.; Johnson, D. G.; Seibert, M.; Govindjee. *Proc. Natl. Acad. Sci. USA* **1989**, *86*, 524.
(19) Wasielewski, M. R.; Johnson, D. G.; Govindjee; Preston, C.; Seibert, M. *Photosynth. Res.* **1989**, *22*, 89.
(20) Schatz, G. H.; Brock, H.; Holzwarth, A. R. *Proc. Natl. Acad. Sci. USA* **1987**, *84*, 8414.
(21) Schatz, G. H.; Brock, H.; Holzwarth, A. R. *Biophys. J.* **1988**, *54*, 397.
(22) Roelofs, T. A.; Gilbert, M.; Shuvalov, V. A.; Holzwarth, A. R. *Biochim. Biophys. Acta* **1991**, *1060*, 237.
(23) Roelofs, T. A.; Kwa, S. L. S.; van Grondelle, R.; Dekker, J. P.; Holzwarth, A. R. *Biochim. Biophys. Acta* **1993**, *1143*, 147.
(24) Holzwarth, A. R.; Müller, M. G.; Gatzen, G.; Hucke, M.; Griebenow, K. *J. Lumin.* **1994**, *60/61*, 497.
(25) Hastings, G.; Durrant, J. R.; Barber, J.; Porter, G.; Klug, D. R. *Biochemistry* **1992**, *31*, 7638.
(26) Schelvis, J. P. M.; van Noort, P. I.; Aartsma, T. J.; van Gorkom, H. J. *Biochim. Biophys. Acta* **1994**, *1184*, 242.
(27) Jankowiak, R.; Tang, D.; Small, G. J.; Seibert, M. *J. Phys. Chem.* **1989**, *93*, 1649.
(28) Tang, D.; Jankowiak, R.; Seibert, M.; Yocum, C. F.; Small, G. J. *J. Phys. Chem.* **1990**, *94*, 6519.
(29) Rech, T.; Durrant, J. R.; Joseph, D. M.; Barber, J.; Porter, G.; Klug, D. R. *Biochemistry* **1994**, *33*, 14768.
(30) Durrant, J. R.; Hastings, G.; Joseph, D. M.; Barber, J.; Porter, G.; Klug, D. R. *Biochemistry* **1993**, *32*, 8259.
(31) van Leeuwen, P. J.; Nieveen, M. C.; van de Meent, E. J.; Dekker, J. P.; van Gorkom, H. J. *Photosynth. Res.* **1991**, *28*, 149.
(32) Roelofs, T. A.; Lee, C.-H.; Holzwarth, A. R. *Biophys. J.* **1992**, *61*, 1147.
(33) Müller, M. G.; Griebenow, K.; Holzwarth, A. R. *Chem. Phys. Lett.* **1992**, *199*, 465.
(34) Müller, M. G.; Drews, G.; Holzwarth, A. R. *Biochim. Biophys. Acta* **1993**, *1142*, 49.
(35) Holzwarth, A. R. In *Biophysical Techniques. Advances in Photosynthesis Research*; Amesz, J., Hoff, A., Eds.; 1995.
(36) Livesey, A. K.; Brochon, J.-C. *Biophys. J.* **1987**, *52*, 693.
(37) Durrant, J. R.; Hastings, G.; Hong, Q.; Barber, J.; Porter, G.; Klug, D. R. *Chem. Phys. Lett.* **1992**, *188*, 54.
(38) Crystall, B.; Booth, P. J.; Klug, D. R.; Barber, J.; Porter, G. *FEBS Lett.* **1989**, *249*, 75.
(39) Booth, P. J.; Crystall, B.; Ahmad, I.; Barber, J.; Porter, G.; Klug, D. R. *Biochemistry* **1991**, *30*, 7573.
(40) Govindjee; van de Ven, M.; Preston, C.; Seibert, M.; Gratton, E. *Biochim. Biophys. Acta* **1990**, *1015*, 173.
(41) Roelofs, T. A.; Holzwarth, A. R. *Biophys. J.* **1990**, *57*, 1141.
(42) Schweitzer, G.; Hucke, M.; Griebenow, K.; Müller, M. G.; Holzwarth, A. R. *Chem. Phys. Lett.* **1992**, *190*, 149.
(43) Marquardt, D. W. *J. Soc. Ind. Appl. Math.* **1963**, *11*, 431.
(44) Kwa, S. L. S.; Tilly, N. T.; Eijckelhoff, C.; van Grondelle, R.; Dekker, J. P. *J. Phys. Chem.* **1994**, *98*, 7712.
(45) Michel, H.; Deisenhofer, J. *Biochemistry* **1988**, *27*, 1.
(46) Ruffle, S. V.; Donnelly, D.; Blundell, T. L.; Nugent, J. H. *Photosynth. Res.* **1992**, *34*, 287.
(47) Nugent, J. H.; Ruffle, S. V.; Berry, M. C. *Biochem. Soc. Trans.* **1993**, *21*, 22.
(48) Trinkunas, G.; Holzwarth, A. R. *Biophys. J.* **1994**, *66*, 415.
(49) Müller, M. G.; Hucke, M.; Reus, M.; Holzwarth, A. R. *J. Phys. Chem.*, in press.
(50) Parson, W. W. In *Chlorophylls*; Scheer, H. Ed.; CRC Press: Boca Raton, 1991; p 1153.
(51) Gatzen, G.; Griebenow, K.; Müller, M. G.; Holzwarth, A. R. In *Research in Photosynthesis, II*; Murata, N., Ed.; Kluwer Academic Publishers: Dordrecht, The Netherlands, 1992; p 69.
(52) Holzwarth, A. R.; Roelofs, T. A. *J. Photochem. Photobiol. B* **1992**, *15*, 45.
(53) Crystall, B.; Booth, P. J.; Barber, J.; Klug, D. R.; Porter, G. In *Current Research in Photosynthesis*; Baltscheffsky, M., Ed.; Kluwer Academic Publishers: Dordrecht, The Netherlands, 1990; p 455.
(54) Peloquin, J. M.; Williams, J. C.; Lin, X.; et al. *Biochemistry* **1994**, *33*, 8089.
(55) Müller, M. G.; Dorra, D.; Holzwarth, A. R.; Gad'on, N.; Drews, G. In *Photosynthesis: from Light to Biosphere. Proceedings of the Xth International Photosynthesis Congress*, Montpellier, 1995; Mathis, P., Ed.; Kluwer Academic Publishers: Dordrecht, The Netherlands, 1995; Vol. I, p 595.
(56) Gatzen, G.; Holzwarth, A. R. Unpublished results, 1994.
(57) Gatzen, G.; et al. Manuscript in preparation.

JP9530865